

# The Life and Death of “Bare” Viscous Bubbles

G. Debrégeas, P.-G. de Gennes, F. Brochard-Wyart

Air bubbles collect and explode at the surface of many viscous liquids, as observed with polymer foams, in glass furnaces, and during volcanic eruptions. The liquid film separating the bubble from bulk air can have a long lifetime (if it is viscous) even if it is not protected by a surfactant. These “bare” films display unusual dynamic behaviors in drainage and rupture. Two different model systems were studied: a polymer melt (silicone oil) and a molten (borosilicate) glass of comparable viscosity. Although the two systems differ greatly in their relaxation time, they are described by the same set of laws, which can be understood from a relatively simple hydrodynamic model.

Foams, especially surfactant-stabilized liquid films, play both useful and detrimental roles in industrial processes (1). Foams and bubbles are usually dynamic structures. In a single soap bubble, aging is controlled by the drainage of a water film between two surfactant monolayers. One might expect this to occur by Poiseuille laminar flows between the monolayers acting like fixed walls. In practice, as shown by Mysels *et al.* and others (2), vertical water films drain by turbulent processes: thin regions go up and thick regions go down. This process is similar to the heating of a room by a radiator, where plumes of hot air build up. If a soap film is punctured, the hole radius grows at constant velocity (3), and a rim of liquid forms around the hole. This kinetics results from a balance between the surface energy and the kinetic energy of the rim.

Liquid films can also be produced from highly viscous liquids in the absence of surfactant. These “bare films” can have dramatic effects in glass furnaces, where a large amount of gas (up to 25 kg/m<sup>3</sup>) has to be evacuated from the melt. Similar processes are observed with certain lavas during volcanic eruptions (4).

We studied the bursting kinetics of bare films that were prepared from high-molecular weight silicone oil (by solvent evaporation) and attached to a frame. These films, of thickness  $h \sim 10 \mu\text{m}$ , were stable for several minutes. If they were punctured, the resulting hole grew exponentially with time (5). This unusual kinetics is the signature of a weak dissipation associated with a small shear rate  $s \approx \dot{R}/R$ , where  $R$  is the hole radius and  $\dot{R}$  is the growth velocity.

We report here measurements of drainage and the bursting of air bubbles settling at the free surface of a pure, viscous liquid.

We used a polydimethylsiloxane melt (PDMS) of molecular weight 308,000 and viscosity  $10^3 \text{ Pa}\cdot\text{s}$  (a million times the viscosity of water) at room temperature. We also report measurements of the hole-opening kinetics in borosilicate glass slides heated above the glass temperature.

An air bubble of volume 0.1 to 10 cm<sup>3</sup> was injected at the bottom of a petri dish filled with PDMS. Once a bubble reached the surface (Fig. 1A), its radius  $R_{\text{cap}}$  [measured with a CCD (charge-coupled device) camera] was of order 4 to 16 mm, much larger than the capillary length  $\kappa^{-1} = \sqrt{\gamma/\rho g} \approx 1 \text{ mm}$  ( $\gamma = 21 \text{ mN/m}$  is the surface tension,  $\rho$  is the liquid density, and  $g$  is the gravitational acceleration). In this regime, the protruding cap was essentially a hemisphere of radius  $R_{\text{cap}}$ . The film thickness  $h$  at the top of the bubble was monitored by interferometry using a He-Ne laser source. The interference pattern indicated that the film shape was axisymmetric with the minimum thickness at the top.

The decrease of  $h$  with time  $t$  for two values of  $R_{\text{cap}}$  is shown in Fig. 1B. For  $0.2 \mu\text{m} < h < 10 \mu\text{m}$ , we found an exponential thinning of the film in the form

$$h = h_0 \exp(-t/\tau) \quad (1)$$

with rate  $1/\tau$  proportional to  $R_{\text{cap}}$  (Fig. 1C).

These results can be explained as follows. In the absence of a surfactant, the flow in the film is a plug flow with a velocity field ruled by  $v = v(\theta) = (\rho g R_{\text{cap}}^2 / 2\eta) \sin\theta$  ( $\theta$  being the latitude measured from the pole, and  $\eta$  is the viscosity). Writing the conservation equation,  $\dot{h} + \text{div}(hv) = 0$ , one finds a self-similar solution in the form

$$h(\theta, t) = \frac{h(0,0)}{\cos^4(\theta/2)} \exp(-t/\tau) \quad (2)$$

with

$$\frac{1}{\tau} = \frac{\rho g R_{\text{cap}}}{\eta} \quad (3)$$

in good agreement with the data of Fig. 2 over two decades. Systematic deviations from the exponential law at the early stages of drainage were observed and probably reflect a departure from our postulated self-similar solution in the initial state when the

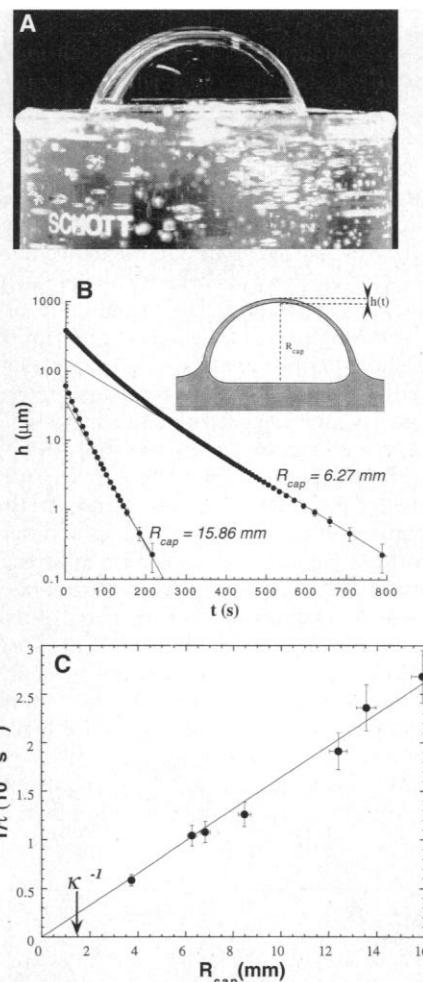


**Fig. 1.** (A) Air bubble settling at the free surface of a PDMS bath of viscosity  $10^3 \text{ Pa}\cdot\text{s}$  (molecular weight  $M_w = 308,000$ ). The volume of the air bubble is 10 ml. Its final hemispherical shape, observed from the side with a CCD camera, was reached within a few seconds after injection. The profile remained unchanged until spontaneous breakup 2 to 20 min later. The radius  $R_{\text{cap}}$  of the hemisphere was determined by image analysis. The interferometric thinning measurements were performed after the bubble reached this final configuration. (B) Time evolution of the thickness  $h$  of the protruding cap, measured at the pole of the bubble, for two values of  $R_{\text{cap}}$ . Exponential thinning is observed in the range  $0.225 \mu\text{m} < h < 10 \mu\text{m}$  (straight line). For each volume of air injected—that is, for each value of  $R_{\text{cap}}$ —the thinning characteristic frequency  $1/\tau = -d(\ln h)/dt$  is extrapolated from measurements of  $h(t)$  in this range. (C) The thinning frequency  $1/\tau$  varied linearly with  $R_{\text{cap}}$ . The arrow on the x axis indicates the value of the capillary length  $\kappa^{-1}$ . In this set of experiments ( $R_{\text{cap}} > \kappa^{-1}$ ), the drainage was driven by gravity.

G. Debrégeas, James Frank Institute, University of Chicago, Chicago, IL 60637, USA.  
P.-G. de Gennes, Ecole Supérieure de Physique et de Chimie Industrielles de la Ville de Paris, 10, rue Vauquelin, 75231 Paris Cedex 05, France.  
F. Brochard-Wyart, Institut Curie, 26, rue d’Ulm, 75248 Paris Cedex 05, France.

film was formed. The crucial feature of these systems without any surfactant sheet is that the velocity gradients were of order  $v/R_{\text{cap}}$  instead of  $v/h$ . The dissipation was thus weak, which resulted in surprisingly high drainage rates for such viscous bubbles.

Spontaneous breakup of the bubble generally occurred when  $h \sim 70$  nm. At this thickness, long-range van der Waals interactions tend to enhance the film thinning. A hole spontaneously formed at the top of the bubble and then rapidly expanded. The bursting velocity was then greater than 10 m/s and did not allow any accurate measurement. To get a quantitative insight, we punctured the bubble at the pole at different stages of the drainage, when the thickness  $h$ , estimated using the Newton's rings that showed up during the last stages of the drainage, ranged between 200 nm and a few micrometers. In this particular experiment, the volume of air injected was kept identical (10 ml), corresponding to  $R_{\text{cap}} = 1.7$  cm. The rupture was monitored with a high-speed camera (1000 frames per second) (Fig. 2A). Up to a radius  $R \sim 2$  mm, the hole grew exponentially with time (Fig. 2B). This result is in agreement with our earlier findings on flat film (5), where the hole radius obeyed

$$R = R_0 \exp\left(\frac{\gamma t}{\eta h}\right) \quad (4)$$

Equation 4 can be understood from a "soft balloon" model. Viscoelasticity is important here. In conventional (Newtonian) liquid films, when a hole opens, the corresponding amount of liquid collects into a circular rise around the hole. The growth velocity  $V$  is controlled by a balance between capillary and inertial (or viscous) forces: it does not vary during growth. For instance, in viscous regime,  $V \sim C\gamma/\eta$  ( $C$  is a constant).

Our liquids were different. At short times, they behaved like rubbers with a shear modulus  $\mu$ . For slow processes, they flowed with a large viscosity  $\eta = \mu T_r$ , where  $T_r$  is a terminal relaxation time (of order 10 ms for our silicone oils). When a hole opened in our silicone film, the Laplace pressure  $2\gamma/h$  acting at the periphery of the hole was elastically propagated outward at a velocity  $2c$ , where  $c = (\mu/\rho)^{1/2}$  is the velocity of transverse shear waves (6). For an infinite plane film, the radial elastic stress component at a distance  $r$  from the center of the hole is

$$\sigma_r = -\frac{2\gamma}{h} \left(\frac{R}{r}\right)^2 \quad (5)$$

The stress  $\sigma_r$  varies with a typical frequency of order  $\dot{R}/R \ll 1/T_r$ . The flows  $v(r)$  induced in the film thus correspond to a purely viscous response described by

$$\sigma_r = 2\eta \frac{\partial v}{\partial r} \quad (6)$$

Integration of Eq. 6 using Eq. 5 yields a flow field

$$v = v(r) = \frac{\gamma}{\eta h} \frac{R^2}{r} \quad (7)$$

Writing  $\dot{R} = v(R)$ , one can finally derive the exponential growth law of Eq. 4.

For our present experiment, this description remained valid as long as the hole radius  $R$  was small compared to the extension of the top region of the bubble, where the film was almost flat and uniform in thickness. Bubble bursting demonstrated the striking effect of a short time elasticity on thin liquid film rupture. The viscous dissipation was greatly reduced, and bursting velocities were enhanced by a factor  $R/h$ : the maximum observed velocities  $\dot{R}$  were thus in the range from 10 to 100 cm/s, that is, up to  $10^4$  times the velocity expected for a Newtonian liquid of same viscosity.

At large  $R$ , however, the bursting slowed down because the hole met progressively thicker film. Simultaneously, a crumpling instability appeared as the bubble deflated and fell under its own weight: once punctured, the overpressure that previously maintained the hemispherical shape was released. This "parachute instability" (Fig.

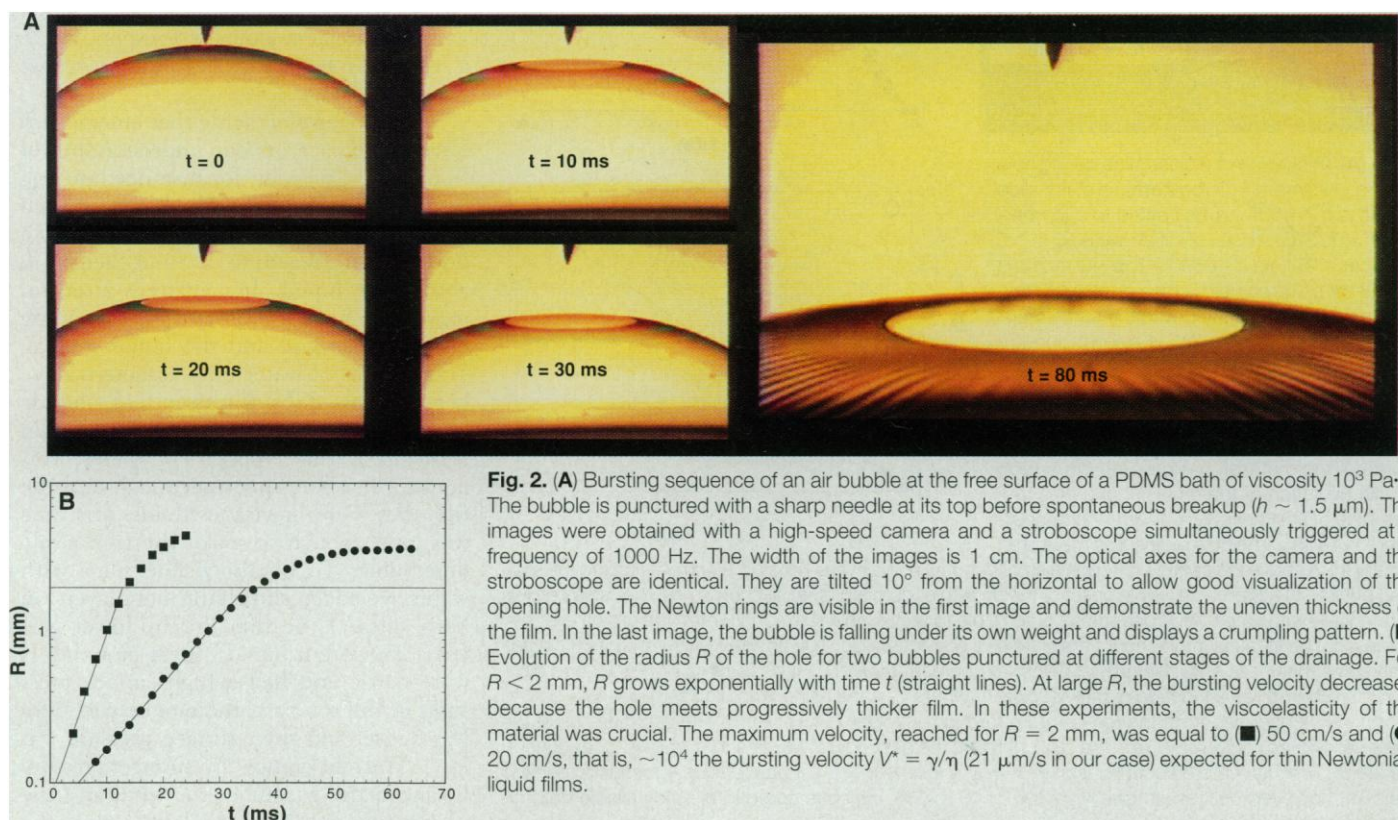


**Fig. 2.** (A) Bursting sequence of an air bubble at the free surface of a PDMS bath of viscosity  $10^3$  Pa·s. The bubble is punctured with a sharp needle at its top before spontaneous breakup ( $h \sim 1.5$   $\mu\text{m}$ ). The images were obtained with a high-speed camera and a stroboscope simultaneously triggered at a frequency of 1000 Hz. The width of the images is 1 cm. The optical axes for the camera and the stroboscope are identical. They are tilted  $10^\circ$  from the horizontal to allow good visualization of the opening hole. The Newton rings are visible in the first image and demonstrate the uneven thickness of the film. In the last image, the bubble is falling under its own weight and displays a crumpling pattern. (B) Evolution of the radius  $R$  of the hole for two bubbles punctured at different stages of the drainage. For  $R < 2$  mm,  $R$  grows exponentially with time  $t$  (straight lines). At large  $R$ , the bursting velocity decreases because the hole meets progressively thicker film. In these experiments, the viscoelasticity of the material was crucial. The maximum velocity, reached for  $R = 2$  mm, was equal to (■) 50 cm/s and (●) 20 cm/s, that is,  $\sim 10^4$  the bursting velocity  $V^* = \gamma/\eta$  (21  $\mu\text{m/s}$  in our case) expected for thin Newtonian liquid films.

2A) has not yet been studied in detail. We present here a tentative picture and an estimate of the characteristic wavelength  $\chi$ . The idea is again that the liquid sheet, at short times, behaves like an elastic plate with a certain rigidity  $K$  (proportional to  $\mu h^3$ ). The unbalanced hydrostatic pressure  $\rho g R$  results in an apparent negative surface tension  $\tilde{\gamma} = \rho g R h$ . The characteristic wavelength for a buckling instability is then  $\xi = (K/\tilde{\gamma})^{1/2}$ : this expression gives the right order of magnitude, but the  $R$  and  $h$  dependence of  $\xi$  remains to be checked. The corrugation eventually disappears because of viscous flows as the hole slowly progresses toward the thick edge of the film.

The bursting kinetics of glassy liquid films has also been addressed with the use of borosilicate slides of thickness  $h_0 = 143$  or  $537 \mu\text{m}$ . A hole of radius  $R_0 \sim 1$  mm was drilled in the center of each slide. The slab was held on a fireproof clay support, leaving the central part (diameter  $2L = 4$  cm) self-supported. It was then put into an oven; a small rectangular window allowed measurement of the hole radius  $R(t)$  after

melting (at temperature  $T$ ). The time required for the slide to reach the final temperature was of order 3 min (7). Some values of the viscosity  $\eta$  at low  $T$  were obtained from the glass manufacturer, and values at higher  $T$  were then extrapolated with the use of a standard Volger-Fulcker form. We focused on  $T < 812^\circ\text{C}$ , corresponding to  $\eta > 10^6$  Pa.s. In the range of temperature and slide thickness explored, we observed hole-opening velocities  $\dot{R} \sim 1$  to  $100 \mu\text{m/s}$ .

We were able to interpret the early moments of the hole-opening process within the same theoretical scheme. However, to maintain the validity of the model at later stages of the rupture, we had to introduce two modifications to account for the finite size of the sample. To calculate the stress field in the film, we imposed a “no displacement” condition at  $r = L$  (the glass is there intimately stuck to the support). Equation 5 thus becomes

$$\sigma_{rr} = -\frac{2\gamma}{h} \left(\frac{R}{r}\right)^2 \frac{1 + (r/L)^2}{1 + (R/L)^2} \quad (8)$$

We also incorporated the homogeneous thickening of the film corresponding to a constant volume of liquid in the suspended part. The thickness  $h$  is then time dependent

$$h(t) = h_0 \frac{L^2}{L^2 - R(t)^2} \quad (9)$$

We actually checked the flatness of the remaining film and measured its thickness  $h(t)$  by a simple trick: we stopped the growth at a certain time  $t$  [and radius  $R(t)$ ] by quenching. The sample then broke, but we could recover the pieces and study their profile (Fig. 3A). This measurement confirmed the thickening law (Eq. 9).

Equations 6, 8, and 9 finally yield the following differential equation for the hole growth kinetics (equivalent to Eq. 4 when  $R/L$  tends to 0)

$$v(R) = \frac{dR}{dt} = \frac{R [1 - (R/L)^2]^2}{\tau_1 [1 + (R/L)^2]} \quad (10)$$

with

$$\tau_1 = \eta h_0 / \gamma \quad (11)$$

These equations give a good description of the observed hole-opening dynamics in the range of thicknesses and viscosities studied (Fig. 3, B and C).

The validity of the soft-balloon model for both polymer and mineral glasses is a nontrivial result, because the viscoelastic features of these two systems are very different: for instance, at one particular viscosity, the polymer system has a much weaker Plateau modulus (corresponding to a rubberlike behavior) than the inorganic glass.

The concepts on aging that emerge also have an impact on our understanding of film birth. Consider, for instance, an “egg beater” experiment, in which a horizontal piece of wire is quickly pulled out of a liquid bath, reaching a final height  $L$  above the liquid. Immediately after removal, we have a “young film” extending between the wire and the liquid surface. Young films of water plus surfactant have been discussed by Lucassen (1) and de Gennes (8). Without surfactant, the film thins in a time  $\eta/\rho g L$ . For water, this duration is short (microseconds), and the film dies. For our viscous fluids, this time was long enough to make the film easily observable. To obtain visible films with water, we added surfactant monolayers on both sides of the film. In the lower part (near the parent liquid), these monolayers were dense and had a high surface pressure; in the top part, the monolayers were less dense, and their surface pressure was low. This difference in surface pressure balanced the weight of the film, and the young film survived. At later times, the

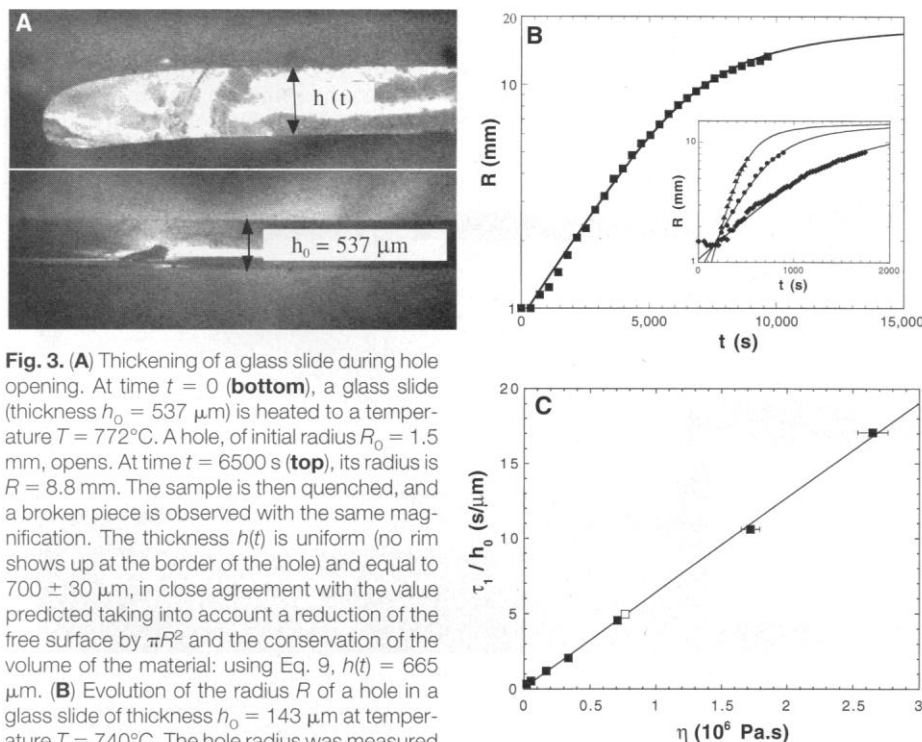


**Fig. 3.** (A) Thickening of a glass slide during hole opening. At time  $t = 0$  (bottom), a glass slide (thickness  $h_0 = 537 \mu\text{m}$ ) is heated to a temperature  $T = 772^\circ\text{C}$ . A hole, of initial radius  $R_0 = 1.5$  mm, opens. At time  $t = 6500$  s (top), its radius is  $R = 8.8$  mm. The sample is then quenched, and a broken piece is observed with the same magnification. The thickness  $h(t)$  is uniform (no rim shows up at the border of the hole) and equal to  $700 \pm 30 \mu\text{m}$ , in close agreement with the value predicted taking into account a reduction of the free surface by  $\pi R^2$  and the conservation of the volume of the material: using Eq. 9,  $h(t) = 665 \mu\text{m}$ . (B) Evolution of the radius  $R$  of a hole in a glass slide of thickness  $h_0 = 143 \mu\text{m}$  at temperature  $T = 740^\circ\text{C}$ . The hole radius was measured optically from above the sample, through a small window in the oven. Time  $t = 0$  corresponds to the slide being put into the oven. The visible onset of the growth occurs at 200 s. At short times, the radius grows exponentially with time  $t$ . As  $R$  becomes comparable to the sample size  $L = 20$  mm, the growth velocity decreases. The fit takes into account the finite size correction (Eq. 10). (Inset) Measurements for slides of the same thickness  $h_0 = 143 \mu\text{m}$  at higher temperatures: ( $\blacktriangle$ )  $T = 812^\circ\text{C}$ , ( $\bullet$ )  $T = 792^\circ\text{C}$ , and ( $\blacklozenge$ )  $T = 772^\circ\text{C}$ . (C)  $\tau_1/h_0$  as a function of the viscosity  $\eta$ , where  $\tau_1$  is the rising time of the exponential growth at short  $t$ ;  $\eta$  is deduced from the temperature through a Volger-Fulcker form. The thickness  $h_0$  of the slide is ( $\blacksquare$ )  $143 \mu\text{m}$  or ( $\square$ )  $537 \mu\text{m}$ . The straight line is the best power-law fit and gives a 1.02 exponent. This result confirms the predicted relation  $\tau_1 = \eta h_0 / \gamma$  (Eq. 11). The surface tension  $\gamma$  for this material is unknown; however, our results give  $\gamma = 200 \pm 10$  mN/m, which is comparable to available data on borosilicate glass (10).

film drained but the flows were confined between fixed walls, and so the drainage was slow.

Our polymer films were "bare": There were no surfactants added and no pollution (such as proteins on water films or dust particles). The trick was to use a liquid of very low surface tension (such as silicones or fluorinated chains): Pollutants do not adsorb easily on these surfaces.

A final remark on the death of our films: The detailed viscoelastic properties of our materials did not show up in our systems. However, the existence of a high-frequency regime where the material behaves like an elastic solid (of shear modulus  $\mu$ ) is crucial. It enables the propagation of the Laplace stress up to a distance  $2cT_r$ . One common and essential feature of our systems is that  $cT_r$  was larger than the sample size.

The present experiments focused on two model systems: linear polymer melts

and conventional glasses. However, our findings may be transposed to other viscoelastic systems, for instance, physical gels with no permanent cross-links and possibly the cytoskeletons, such as the spectrin network of red blood cells and other biological gels (9).

#### REFERENCES AND NOTES

1. For a review, see J. Lucassen, in *Anionic Surfactants* (Dekker, New York, 1981).
2. K. Mysels, K. Shinoda, S. Frenkel, *Soap Films* (Pergamon, London, 1959); D. Weaire, N. Pittet, S. Hutzler, *Phys. Rev. Lett.* **71**, 2670 (1993); E. Ruckenstein and A. Bhakta, *Langmuir* **11**, 1486 (1995).
3. For a review, see P.-G. de Gennes, *Faraday Discuss.* **104**, 1 (1996).
4. M. T. Mangau and K. V. Cashman, *J. Volcanol. Geotherm. Res.* **73**, 1 (1996).
5. G. Debregas, P. Martin, F. Brochard-Wyart, *Phys. Rev. Lett.* **75**, 3886 (1995).
6. See, for instance, L. D. Landau and E. M. Lifshits, *Theory of Elasticity* (Pergamon, London, 1959), chap. 25, p. 110. The velocity  $2c$  is expected when the Lamé coefficients  $\lambda$  and  $\mu$  satisfy  $\mu \ll \lambda$ .
7. The time required for the slide to reach its final temperature cannot be easily determined. However, we noted that the visible onset of the hole opening was systematically of order 200 s. By limiting our observations to relatively low temperatures ( $T < 812^\circ\text{C}$ ), we could decouple this delay and the characteristic time for hole opening (on the order of 15 min to 2 hours). The rapid decrease of the viscosity with decreasing temperature makes the onset of the growth process sharp (Fig. 3A) and indicates that the whole measurement is done at a constant temperature. The biggest uncertainty comes from fluctuations in the oven temperature, which are of the order of  $\pm 0.5^\circ\text{C}$ .
8. P.-G. de Gennes, *C. R. Acad. Sci. Ser. II* **305**, 9 (1987).
9. M. Lindemann, M. Steinmetz, M. Winterhalter, *Prog. Colloid Polym. Sci.* **105**, 209 (1997).
10. R. H. Doremus, *Glass Science* (Wiley, New York, ed. 2, 1995), chap. 11.
11. Bursting experiments on viscous bubbles were performed at Rhône-Poulenc Research (St. Fons, France). We thank L. Vovelle and J. J. Martin for their help. We would like to acknowledge the support of H. Aribart and S. Creux, from the CNRS–St. Gobain research laboratory (Aubervilliers, France), where the experiments on glass slides were done. We are grateful to A. Buguin, R. Fondecave, and P. Martin for fruitful comments on this work.

20 October 1997; accepted 2 February 1998

## Deuterium in Comet C/1995 O1 (Hale-Bopp): Detection of DCN

Roland Meier,\*† Tobias C. Owen,\* David C. Jewitt,\* Henry E. Matthews, Matthew Senay,\* Nicolas Biver, Dominique Bockelée-Morvan, Jacques Crovisier, Daniel Gautier

Deuterated hydrogen cyanide (DCN) was detected in a comet, C/1995 O1 (Hale-Bopp), with the use of the James Clerk Maxwell Telescope on Mauna Kea, Hawaii. The inferred deuterium/hydrogen (D/H) ratio in hydrogen cyanide (HCN) is  $(D/H)_{\text{HCN}} = (2.3 \pm 0.4) \times 10^{-3}$ . This ratio is higher than the D/H ratio found in cometary water and supports the interstellar origin of cometary ices. The observed values of D/H in water and HCN imply a kinetic temperature  $\geq 30 \pm 10$  K in the fragment of interstellar cloud that formed the solar system.

We detected deuterated water (HDO) in Comet C/1995 O1 (Hale-Bopp) (1). This detection resulted in the third measurement of the D/H ratio in cometary water, which appears to be essentially the same in Comets P/Halley, C/1996 B2 (Hyakutake), and

Hale-Bopp,  $D/H = (3.16 \pm 0.34) \times 10^{-4}$  (2). If comets have preserved unmodified interstellar material, we expect hydrogen-containing compounds other than  $\text{H}_2\text{O}$  to exhibit different values of D/H, a well-known result of ion-molecule reactions in interstellar clouds (3). We made several attempts to detect DCN in Hale-Bopp, to test this prediction, because HCN exhibits the most prominent emission lines of any hydrogenated species detected in cometary millimeter and submillimeter spectra thus far. Our initial effort was made before perihelion and did not succeed. Here, we report our detection of DCN from observations of Hale-Bopp using the James Clerk Maxwell Telescope (JCMT) on Mauna Kea, Hawaii, near the comet's peak activity and under more favorable atmospheric conditions.

The  $J = 5-4$  rotational transition of DCN at 362.0465 GHz was detected on a

spectrum (Fig. 1) recorded on 28.0 April 1997 (UT). At the time of these observations, Hale-Bopp was about 1 month past perihelion at a heliocentric distance of 1.031 astronomical units (AU) and 1.72 AU distant from Earth.

We obtained the observations with the JCMT using a dual-channel heterodyne receiver ("B3") sensitive to submillimeter radiation, with subsequent signal processing effected with an autocorrelation spectrometer. Sky background emission was removed by frequency switching  $\pm 8.1$  MHz once every 30 s. Receiver B3 uses two low-noise niobium junctions that simultaneously detect orthogonally polarized radiation from the same point on the sky. Radiation incident on B3 is detected in two sidebands separated by 8.0 GHz. By means of a dual-beam interferometer in the beam path within the receiver, the "image" sideband was almost entirely suppressed, and the "signal" sideband was transmitted and the temperature scale well established. We tuned the receiver such that the DCN 5-4 line, arising in the signal sideband, appeared in the spectrum displaced from HCN 4-3, which, at a frequency of 354.5055 GHz, arose in the image sideband. Although the HCN 4-3 line was suppressed by a factor of about 25 by the image sideband rejection, the emission from it allowed us to monitor the quality of the telescope pointing very effectively.

Hale-Bopp was a daytime object during these observations with a solar elongation of only  $33^\circ$ . JCMT is protected by a Gore-Tex wind blind from direct solar radiation, which limits the deformation of the telescope surface due to heating. Pointing and

R. Meier, T. C. Owen, D. C. Jewitt, N. Biver, University of Hawaii, Institute for Astronomy, 2680 Woodlawn Drive, Honolulu, HI 96822, USA.

H. E. Matthews, National Research Council of Canada, Herzberg Institute of Astrophysics, 5071 West Saanich Road, Victoria, BC V8X 4M6, Canada, and Joint Astronomy Centre, 660 North A'Ohoku Place, Hilo, HI 96720, USA.

M. Senay, Five College Radio Astronomy Observatory, University of Massachusetts, Amherst, MA 01003-4517, USA.

D. Bockelée-Morvan, J. Crovisier, D. Gautier, Observatoire de Paris-Meudon, 5 Place Jules Janssen, F-92195 Meudon, Cedex, France.

\*Visiting astronomer at the James Clerk Maxwell Telescope, 600 North A'Ohoku Place, Hilo, HI 96720, USA.

†To whom correspondence should be addressed: E-mail: meier@uhifa.ifa.hawaii.edu